Journal of Molecular Spectroscopy **195,** 177–184 (1999)
Article ID jmsp.1999.7820, available online at http://www.idealibrary.com on IDEAL®

Terahertz Spectroscopy of the Amidogen Radical, NH_2

Holger S. P. Müller,* Henrik Klein,* Sergei P. Belov,* Gisbert Winnewisser,* Isamu Morino,† Koichi M. T. Yamada,† and Shuji Saito‡

*Physikalisches Institut, Universität zu Köln, Zülpicher Str. 77, D-50937 Cologne, Germany; †National Institute for Advanced Interdisciplinary Research, 1-1-4 Higashi, Tsukuba, Ibaraki 305, Japan; and ‡Institute for Molecular Science, Myodaiji, Okazaki 444, Japan

Received November 4, 1998; in revised form January 5, 1999

The rotational spectrum of the NH_2 radical in its $\tilde{X}\,^2B_1$ ground vibronic state was investigated between 614 and 1003 GHz. One hundred fifty-nine newly observed lines (188 hyperfine components) of six rotational transitions with $0 \le N \le 5$ and $0 \le K_a \le 4$ were used in the final, global fit of field-free data for the (000) vibrational state. Recent results from Fourier transform far-infrared (FT-FIR), and millimeter- and submillimeter-wave spectroscopy, as well as microwave optical double resonance (MODR) and recent FIR laser sideband data, were also used in the fit. A large set of spectroscopic constants reproduces the input data within experimental uncertainties and permits the precise prediction of low-N, low-K_a transitions of interest for the astrophysical community. In particular, the astrophysically important 1_{11}–0_{00} transition of ortho NH_2 was observed near 952.57 and 959.50 GHz.

I. INTRODUCTION

The NH_2 radical is an intermediate in the formation of NH_3 from nitrogen atoms as well as in its destruction. Thus, it is an important astrophysical molecule. Its cometary emission spectrum from the first excited to the ground electronic state was observed more than 50 years ago (*1*). Recently, the 1_{10}–1_{01} transition of para-NH_2 has been observed in absorption in interstellar space by submillimeter wave (sub-mmW) spectroscopy toward the Galactic center source Sagittarius B2 (*2*).

The amidogen radical is a very asymmetric, prolate top ($\kappa = -0.384$) with its dipole moment along the b axis. It has C_{2v} symmetry and a $^2B_1$ ground electronic state. Because of the two equivalent hydrogen nuclei ($I_H = \frac{1}{2}$), rotational levels with $K_a + K_c$ even and odd are distinguished as ortho and para spin modification, respectively. NH_2 is a light and floppy molecule, and the rotational energy level scheme shown in Fig. 1 resembles that of H_2O ($\tilde{X}\,^1A_1$). The major difference is that the ortho and para states are exchanged due to the different electronic symmetries of the molecules. The low-N transitions are of particular astrophysical relevance; however, some of them occur at very high frequencies, near 1 THz, for example 1_{11}–0_{00}. The atmospheric opacity in this frequency region can be overcome by using air-borne or satellite-based observatories.

The rotational spectrum of NH_2 is more complex than that of H_2O because of the fine and hyperfine splitting caused by the spin of the unpaired electron ($S = \frac{1}{2}$) and the N nucleus ($I_N = 1$), respectively. Additional hyperfine splitting occurs in the ortho levels due to the spins of the two equivalent H nuclei ($I_{H1} = I_{H2} = \frac{1}{2}$). The splitting of the transition is schematically shown for 1_{11}–0_{00} in Fig. 2.

Amidogen has been subjected to numerous spectroscopic studies. Field-free investigations of the ground vibronic state include microwave optical double resonance (MODR); mostly magnetic dipole transitions between the two electron spin components of a rotational level have been observed (*3–5*). In the mmW and sub-mmW regions, NH_2 has been studied by Charo *et al.* (*6*) and very recently, by Tonooka *et al.* (*7*). Its Fourier transform far-infrared (FT-FIR) spectrum has been reported by Morino and Kawaguchi (*8*). More recently, Ozeki and Saito have investigated its spectrum between 1.3 and 2.5 THz by FIR laser sideband spectroscopy (*9*). A more detailed account on the spectroscopy of amidogen can be found, for example, in Ref. (*7*).

Broadband scanning spectroscopy was extended into the THz region first in 1994 by frequency and phase stabilization of continuously tunable backward-wave-oscillators (BWO) (*10*). The achieved measurement accuracy of the Cologne terahertz spectrometer can be as low as ~1 kHz for isolated strong lines when it is operated in saturation mode (*11*).

In the present study we have measured low-N transitions of the NH_2 radical in the terahertz region with microwave (MW) accuracy. A global analysis of all available field-free pure rotational data in the ground vibronic state has been carried out in order to obtain precise spectroscopic constants for the ground vibronic state, which facilitates the basis for identifying NH_2 lines throughout the MW to FIR regions.

II. EXPERIMENTAL DETAILS

The NH_2 radical was generated by a dc discharge in a mixture of NH_3 and Ar. The typical partial pressures of the

Supplementary data for this article may be found on the journal home page (http://www.academicpress.com/jms).

0022-2852/99 $30.00

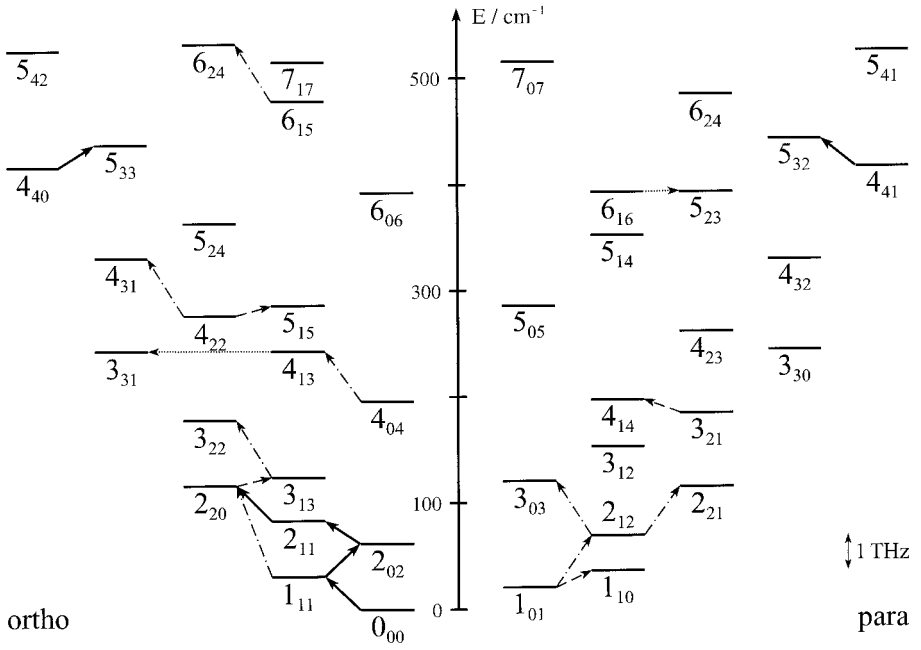

FIG. 1. Part of the rotational energy level diagram of amidogen, NH_2, $\tilde{X}\,^2B_1$. Transitions observed in this and a previous mmW study (*7*) are indicated by arrows with full and dashed lines, respectively. Observed MW transitions involving a change in rotational state (*3–5*) are represented by arrows with dotted lines. The lines observed by laser side band spectroscopy (*9*) are referred to by arrows with dashed–dotted lines. The electron spin–rotation transitions (*3–5*) and transitions observed by FT-FIR (*8*) are not shown.

gases were 12 and 180 mTorr, respectively, monitored by a Baratron gauge. The discharge current was about 120 mA. The two cylinder electrodes made by 0.1-mm-thickness stainless steel sheet were inserted in a 1-m-long, 80 mm i.d. absorption cell with 50-cm distance between each electrode. The conditions were rather similar to the ones used to generate the imidogen radical, NH (*12*). In fact, the two radicals occurred simultaneously during the study of the rotational spectrum of NH with the Cologne terahertz spectrometer between ~0.90 and ~1.01 THz (*12*). The spectra between ~610 and ~790 GHz were recorded at the National Insititute for Advanced Interdisciplinary Research (NAIR), Japan with a sub-mmW spectrometer constructed along the design criteria of the Cologne terahertz spectrometer (*13*).

The spectrometers in both laboratories are essentially the same. The sub-mmW radiation produced by water-cooled BWO's is directed by a feed horn to a mixer-diode. The mixer diode is made by Kölner Observatorium für Submm-Astronomie (KOSMA), the University of Cologne, and is a planar Schottky-barrier diode mounted at the edge of the waveguide through which the local oscillator power operating in the 100-GHz region is supplied. The BWO was frequency stabilized by phase-locking its output to a KVARZ synthesizer, which is fed with a 5 MHz reference signal from a rubidium atomic clock providing a short term relative accuracy of better than 10^{-11}. At NAIR a millimeter-wave phase-locked Gunn oscillator is used as the local source in the present study instead of the synthesizer (*13*). The intermediate frequency produced by the mixer-diode is locked at 350 MHz using a phase-lock-loop (PLL). A wire grid polarizer is used as a beam splitter, and a half of the sub-mmW radiation is directed to an absorption cell. The transmitted radiation is focused on a magnetically tuned liquid-Helium cooled InSb hot electron bolometer. The signal is phase-sensitively detected by a lock-in amplifier with source frequency modulation of 10 kHz, and the spectra in the second derivative form are recorded with the 2*f*-detection mode. For the present measurements, the measurement accuracy is typically 50–100 kHz mainly because of the congested line patterns.

III. OBSERVED SPECTRA AND ANALYSIS

Figure 1 displays the rotational energy levels up to about 500 cm^{-1} ordered in ortho and para states. In addition, it serves to summarize the transitions measured previously, except for the electron spin–rotation transitions and those measured by FT-FIR spectroscopy, together with those observed in the present study. The initial predictions and assignments of the 1_{11}–0_{00}, 2_{02}–1_{11}, and 2_{20}–2_{11} rotational transitions were made using the program and the spectroscopic constants from Ref. (*7*). In general, the lines were found quite close to the predictions, and the assignments were straightforward because of the well-predicted hyperfine patterns. In the initial assignments as well as in the final fits, it was important to use intensity-weighted averages of the components in cases of unresolved lines (*14*). The energy levels for the 1_{11}–0_{00} transition are schematically

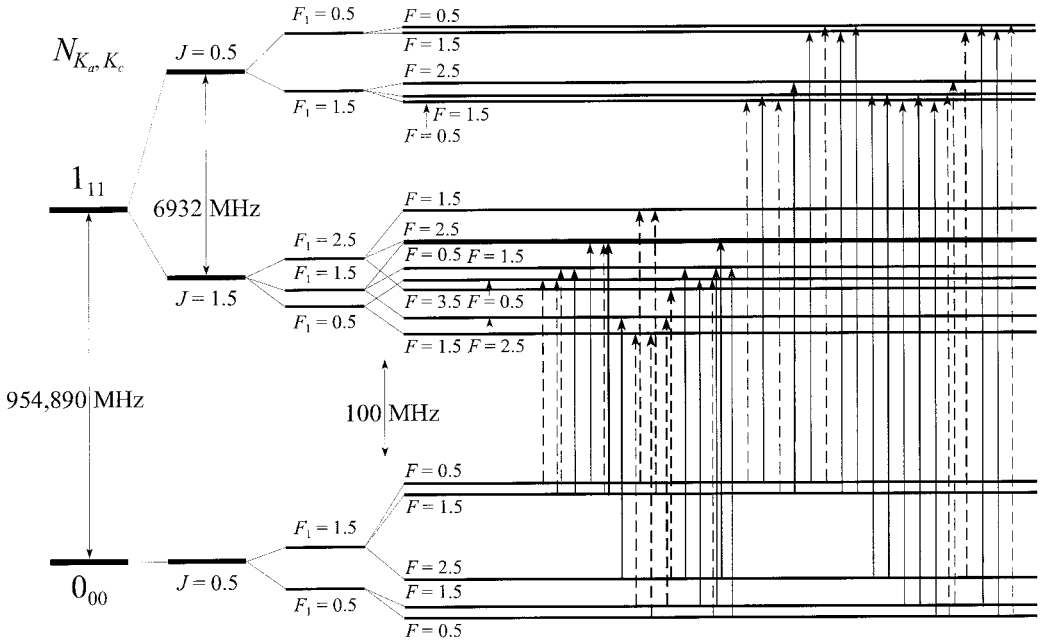

FIG. 2. Energy level diagram for the 1_{11}–0_{00} transition of NH_2. The rotational energy separation as well as the splitting due to the spins of the unpaired electron, the N and H nuclei are indicated by their quantum numbers $N_{Ka,Kc}$, J, F_1, and F, respectively. Note that the scales of the nuclear hyperfine splittings are identical, while the remaining splitting uses different scales. Observed transitions are indicated by arrows; the thickness indicates the relative intensity. Very close arrows indicate overlapping lines; dashed arrows represent lines omitted from the final fit due to unfavorable overlap of hyperfine components, the proximity of stronger lines, or overlap with lines other than NH_2.

shown in Fig. 2. The complexity of the rotational transitions is caused by the combined effects of fine and hyperfine splitting leading to a fairly intricate line pattern. This behavior is exemplarily demonstrated for parts of the two ortho-NH_2 transitions 1_{11}–0_{00} and 2_{11}–2_{02} in Fig. 3. In the case of the 1_{11}–0_{00} transition, the total splitting consists of two fine and about 50 hyperfine structure transitions spread out over a frequency span of 7.2 GHz. Figure 3a shows the lower fine structure component, $J = 1.5 - 0.5$, of this transition which was recorded in Cologne. In Fig. 3b the $J = 1.5 - 1.5$ fine structure component of the 2_{11}–2_{02} Q-branch transition is presented. It was measured at NAIR, and the four fine and about 170 hyperfine structure transitions spread out over 8.0 GHz.

Few blended lines, for which the difference between observed and calculated line positions were more than three times the uncertainties, were omitted from the final fit. These deviations are caused by unfavorable overlap of two or more NH_2 hyperfine components or by overlap with lines other than those of NH_2. One hundred fifty-nine newly observed lines corresponding to 188 hyperfine components were included in the final fit. The newly observed rotational transitions and the number of their fine and hyperfine components used in the final fit are given in Table 1. The list of newly observed transition frequencies, their assignments, uncertainties (mostly 50 or 100 kHz, in some cases up to 250 kHz), and differences between observed frequencies and calculated are available as supplementary data. Among the previously observed MW transitions the ones which involve a change of the rotational state (*3*–*5*) are also inluded while the electron spin–rotation transitions are not in the list. Furthermore, the mmW and sub-mmW transitions from Ref. (*7*) and the laser sideband transitions (*9*) are included. The complete list of transitions used in the final fit as well as predictions of amidogen frequencies, uncertainties, intensities, and assignments in the ground vibronic state are available online in the JPL Submillimeter, Millimeter, and Microwave Line Catalog (http://spec.jpl.nasa.gov) (*15*).

The coupling scheme of the rotational, electron, and the three nuclear spin angular momenta used in the present study follows Refs. (*3*, *7*):

$$\mathbf{N} + \mathbf{S} = \mathbf{J}, \qquad [1]$$

$$\mathbf{J} + \mathbf{I}_N = \mathbf{F}_1, \qquad [2]$$

$$\mathbf{F}_1 + \mathbf{I}_H = \mathbf{F}; \qquad [3]$$

with

$$\mathbf{I}_{H1} + \mathbf{I}_{H2} = \mathbf{I}_H. \qquad [4]$$

The Hamiltonian used for predicting and fitting the NH_2 spectra has the following form:

$$\mathcal{H} = \mathcal{H}_{rot} + \mathcal{H}_{fs} + \mathcal{H}_{hfs}. \qquad [5]$$

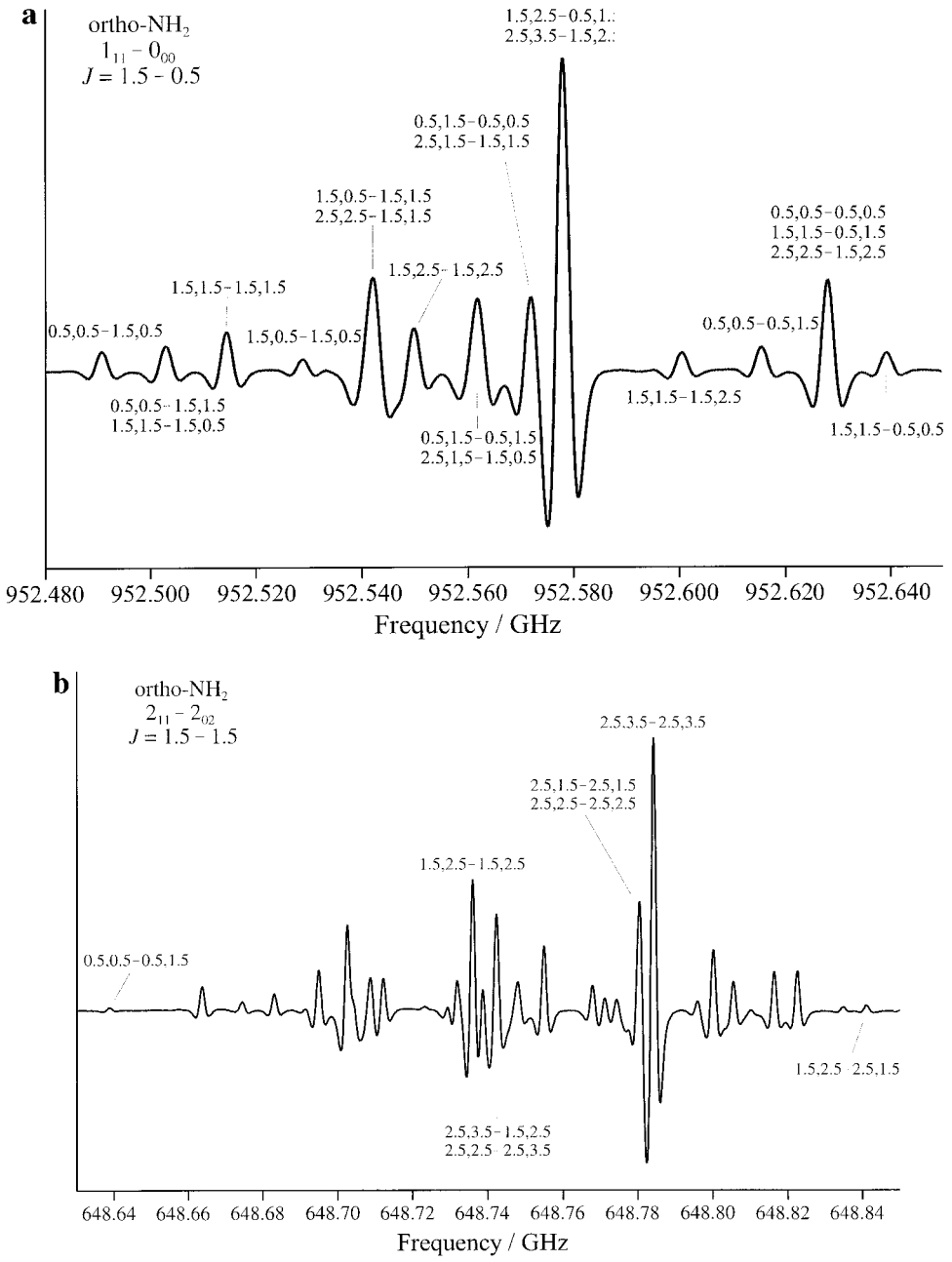

FIG. 3. Hyperfine pattern within one fine structure component of NH_2, $\tilde{X}^2B_1$, shown for two rotational transitions. (a) Detail of the lower fine structure component $J' - J'' = 1.5 - 0.5$ of the rotational transition 1_{11}–0_{00} near 952.57 GHz, recorded in Cologne. (b) Detail of the $J' - J'' = 1.5 - 1.5$ fine structure component of the 2_{11}–2_{02} rotational transition near 648.75 GHz, recorded at NAIR. In trace b the quantum numbers F_1', $F' - F_1''$, F'' are indicated only in part.

where $\mathcal{H}_{\text{rot}}$ is Watson's *A*-reduced rotational Hamiltonian in the I^r representation which contains centrifugal distortion terms up to 12th order. The fine structure Hamiltonian, $\mathcal{H}_{\text{fs}}$, describes the electron spin–rotation (ϵ_{ii}) where up to octic centrifugal distortion terms are included ($\Delta_N^s, \ldots, L_K^s$). The hyperfine Hamiltonian, $\mathcal{H}_{\text{hfs}}$, consists of the following individual contributions:

$$\mathcal{H}_{\text{hfs}} = \mathcal{H}_{\text{ss}}(\text{N}) + \mathcal{H}_{\text{Q}}(\text{N}) + \mathcal{H}_{\text{nsr}}(\text{N}) + \mathcal{H}_{\text{ss}}(\text{H}) + \mathcal{H}_{\text{nsr}}(\text{H}), \quad [6]$$

where $\mathcal{H}_{\text{ss}}$, $\mathcal{H}_{\text{Q}}$, and $\mathcal{H}_{\text{nsr}}$ represent isotropic (a_F) and anisotropic (T_{ij}) spin–spin coupling between the electron spin and the nuclear spins, the nuclear quadrupole coupling (χ_{ii}), and nuclear spin–rotation (C_{ii}) for the N or H nuclei, respectively. Spin–spin coupling between the HH and the NH nuclei, respectively, was insignificantly determined and affected the spectroscopic constants and the standard deviation of the fit only marginally. Therefore, the respective spin–spin coupling constants have been omitted from the final fit.

TABLE 1
Newly Observed Rotational Transitions and Number of Fine and Hyperfine Structure Components Used in the Final Fit

Transition	N_{fs}	N_{hfs}
$5_{33} - 4_{40}$	2	18
$2_{11} - 2_{02}$	4	100
$5_{32} - 4_{41}$	2	6
$2_{02} - 1_{11}$	2	23
$1_{11} - 0_{00}$	2	21
$2_{20} - 2_{11}$	2	20

Pickett's programs SPFIT and SPCAT (*16*) were used for the final assignments and fits of the NH_2 spectra which were performed in Cologne. It should be pointed out that all parameters are positively defined, the quartic centrifugal distortion constants (Δ_N, etc.) being the only exception. The quartic spin–distortion constants are defined positively, as in Brown and Sears (*17*). However, one should pay attention that they were defined negatively in some of the earlier NH_2 studies. In the present study, Δ^s_{KN} and Δ^s_{NK} are found to be highly correlated, as is frequently the case. Since the sum was much better determined than each constant alone, it was used in the final fit instead of Δ^s_{KN}. Sextic spin–distortion terms other than Φ^s_K have been used rarely. A respective Hamiltonian in the *S* reduction has been proposed by Müller *et al.* (*18*). Various combinations of these operators, including off-diagonal elements adjusted for the *A* reduction, were used in trial fits of the data. A satisfactory fit which avoided high correlation utilized $\Phi^s_K N_a^5 S_a + \Phi^s_{NKK}(N^2 N_a^3 S_a + N_a^3 S_a N^2)/2 + \Phi^s_{NNK}(N^4 N_a S_a + N_a S_a N^4)/2$, as well as $L^s_K N_a^7 S_a$, which is the only octic term included in the fit.

Centrifugal corrections on the spin–spin coupling constants were insignificant. Furthermore, the inclusion of the respective constants had only a negligible effect on the standard deviation of the fit. Hence, they were omitted from the final fit. The present data set was not affected by T_{ab}(H), and this constant was kept fixed to the value in Ref. (*19*).

The FT-FIR transitions (*8*) were given uncertainties of 0.0007 cm^{-1} which are based on their weighting relative to the MODR data and based on the resolution of the spectra. Morino and Kawaguchi (*20*) pointed out some typographical errors and misassignments in Ref. (*8*). Some of these misassignments were communicated independently by Vervloet (*21*). They were easily identified using predictions based on the spectroscopic constants reported in that study. The assignments used in the present study were based on these predictions. Since no hyperfine structure was resolved in this study, all lines were treated in the fit accordingly. The mmW and sub-mmW lines measured previously (*7*) were given uncertainties of 50 kHz. The MODR data (mostly transitions between the two electron spin components of a given rotational level, but also one electric dipole-allowed rotational transition, 5_{23}–6_{16}, and one magnetic dipole-allowed rotational transition, 3_{31}–4_{13}) were used with their stated uncertainties (mostly 0.5 MHz, in some cases 1 or 2 MHz) (*3–5*). Initially, the measured FIR laser sideband lines were given uncertainties of 1 MHz as stated by the authors (*9*). However, the average deviation between observed and calculated frequencies was found to be larger than 1 MHz for these lines. A value of 3 MHz was adopted for the uncertainties which was based on the deviations observed for low-*N* transitions which had predicted uncertainties of ~100–300 kHz due to the lines from Ref. (*7*) and from this study. The 5_{32}-5_{23} transition was eliminated from the final fit because of large deviations (~30 MHz) between observed and calculated frequencies which occurred similarly in Ref. (*9*). Throughout the fit, overlapping lines were treated as the intensity–weighted average of the individual components. Recently we have begun to carry out precise NH_2 measurements (~100 kHz) near 2 THz with a frequency stabilized BWO-FIR laser side band system. The results are in good agreement with the predictions from the present study.

The spectroscopic constants are presented in Tables 2–4 together with previous experimental results and values obtained by *ab initio* calculations for some of the hyperfine constants. The dimensionless standard deviation of the fit is 0.845, demonstrating that overall the input data have been reproduced within the assumed experimental uncertainties. Since data of rather different accuracy were used in the present fit, the overall standard deviation is not a sufficient criterion for the quality of the fit, as has been pointed out in Ref. (*23*). Therefore, additional, more detailed, information on the final fit of NH_2 is given in Table 5.

IV. DISCUSSION

The NH_2 radical is light and rather floppy, comparable to H_2O and H_2S. Therefore, a large number of constants are needed to account for the centrifugal distortion effects, including the N_a^{12} constant S_K. The rotational and lower order centrifugal distortion constants as well as the lower order fine structure parameters for the ground vibronic state of NH_2 are in very good agreement with previous values from the FT-FIR study (*8*). The changes in the higher order constants are caused in part by the larger set of distortion terms used in the present study, which resulted in larger uncertainties for some parameters. The agreement between present and previous hyperfine constants is excellent. Some of the uncertainties as well as some of the correlations were reduced by the larger data set. As can be seen in Table 4, high-level *ab initio* calculations are capable of predicting hyperfine constants well. The present results may prompt a more detailed *ab initio* study, which includes effects of quadrupole, nuclear spin–rotation, and nuclear spin–spin coupling, as well.

TABLE 2
Rotational and Centrifugal Distortion Constants[a] (MHz) of NH_2 in Comparison to Previous Values

Parameter	Present	Previously[b]
A	710 302.131 9 (250)	710 305.68 (162)
B	388 288.871 8 (1491)	388 284.24 (60)
C	245 013.954 4 (1316)	245 017.26 (42)
Δ_K	659.765 23 (1561)	659.211 (144)
Δ_{NK}	−125.045 19 (1631)	−124.711 (75)
Δ_N	31.664 38 (428)	31.586 1 (78)
δ_K	29.375 5 (761)	27.605 (33)
δ_N	12.701 85 (208)	12.674 9 (39)
$\Phi_K \cdot 10^3$	1 991.49 (350)	1 956.7 (72)
$\Phi_{KN} \cdot 10^3$	−267.88 (472)	−285.7 (48)
$\Phi_{NK} \cdot 10^3$	−48.98 (139)	−40.23 (81)
$\Phi_N \cdot 10^3$	12.518 3 (1195)	11.347 (51)
$\phi_K \cdot 10^3$	490.64 (778)	243.85 (132)
$\phi_{NK} \cdot 10^3$	−18.655 (1194)	−14.75 (51)
$\phi_N \cdot 10^3$	6.294 3 (432)	5.7515 (243)
$L_K \cdot 10^6$	−10 156. (278)	−9185. (192)
$L_{KKN} \cdot 10^6$	2 472. (290)	3514. (189)
$L_{NK} \cdot 10^6$	−736.9 (1070)	−881. (69)
$L_{NNK} \cdot 10^6$	70.39 (1281)	
$L_N \cdot 10^6$	−4.786 (792)	
$l_K \cdot 10^6$	2 501. (208)	
$l_{KN} \cdot 10^6$	44.3 (432)	
$l_{NK} \cdot 10^6$	45.87 (818)	
$l_N \cdot 10^6$	−3.043 (295)	
$P_K \cdot 10^6$	49.01 (426)	9.38 (102)
$P_{KKN} \cdot 10^6$		15.29 (102)
$P_{KN} \cdot 10^6$		−6.54 (69)
$S_K \cdot 10^6$	−0.184 4 (299)	

[a] Watson's A reduction was used in the representation I^r. Numbers in parenthesis are one standard deviation in units of the least significant figures.
[b] Ref. (*8*).

The hyperfine constants of NH_2 have been discussed to some extent previously (*3*, *7*). In a radical with up to p electrons, the isotropic and anisotropic electron–spin nuclear–spin coupling constants can be used with their atomic values to derive populations of the unpaired electron in s and p valence orbitals, respectively. Taking atomic values for N from Ref. (*24*) and neglecting second order effects, one obtains a spin density of ~0.8 in the out-of-plane 2p orbital at N and very small densities in the 2s and remaining 2p orbitals. This is in agreement with amidogen being a π-radical with a $^2B_1$ electronic ground state. It was pointed out in Ref. (*7*) that the H nuclear spin–rotation coupling constants are usually small and negative, in contrast to most other molecules involving nuclei with positive magnetic moment. The NH_2 values of C_{bb}(H) and C_{cc}(H), obtained here for the first time, are in agreement with this picture. In contrast, the large positive value for C_{aa}(H) is unusual; it indicates, together with a large value of C_{aa}(N), the presence of low-lying electronic states in NH_2 (*7*). The magnitude of C_{aa}(H) was related approximately to the magnitudes of the T_{ii}(H) (*7*).

The present spectroscopic constants allow precise predictions of transition frequencies for a large range of quantum numbers. For example, all transitions with $N \leq 5$ have a predicted uncertainty of about 1 MHz or less with the exceptions of 5_{41}–5_{32} and 5_{42}–5_{33} at ~2.48 and ~2.64 THz, respectively, where the uncertainties are ~1.6 MHz. Because of the large centrifugal distortion effects present in NH_2, the predicted uncertainties of rotational transitions should be viewed cautiously, in particular for those involving N and K_a quantum numbers outside the range of lines used in the present fit.

Finally, a comment concerning the astrophysical detection of NH_2 *via* the lowest N transition 1_{11}–0_{00} may be timely. The transition frequency near 1 THz requires aircraft (e.g., the Stratospheric Observatory for Infrared Astronomy, SOFIA) or satellite measurements to reduce the atmospheric opacity which excludes ground-based observations. From the size of the permanent dipole moment, 1.82 D (*25*), one can expect to observe this transition in emission in dense regions with H_2 density of 10^5–10^6 cm^{-3} provided NH_2 is chemically stable.

TABLE 3
Fine Structure Constants [a] (MHz) of NH_2 in Comparison to Previous Values

Parameter	Present	Previously[b]
ϵ_{aa}	−9 267.972 1 (325)	−9266.58 (33)
ϵ_{bb}	−1 354.273 9 (215)	−1354.939 (147)
ϵ_{cc}	12.292 5 (237)	12.145 (84)
Δ^s_K	34.119 9 (122)	32.638 (123)
$\Delta^s_{KN} + \Delta^s_{NK}$	−3.503 4 (89)	−3.202 1 (252)
Δ^s_{NK}	0.665 (116)	
Δ^s_N	0.316 64 (62)	0.325 99 (183)
δ^s_K	0.549 5 (63)	0.602 6 (201)
δ^s_N	0.160 580 (294)	0.162 91 (99)
$\Phi^s_K \cdot 10^3$	−179.62 (169)	−98.90 (153)
$\Phi^s_{NKK} \cdot 10^3$	7.02 (222)	
$\Phi^s_{NNK} \cdot 10^3$	3.383 (287)	
$L^s_K \cdot 10^3$	0.728 1 (267)	

[a] Electron spin-rotation coupling constants, as well as quartic, some sextic, and one octic distortion constants. See also footnote to Table 2.
[b] Ref. (*8*).

TABLE 4
Hyperfine Structure Constants[a] (MHz) of NH_2 in Comparison to Previous Values

Parameter	Present	Previously[b]	*ab initio*[c]
a_F(N)	28.050 2 (106)	28.061 (17)	24.1
T_{aa}(N)	−43.188 1 (173)	−43.035 (30)	−42.4
T_{bb}(N)	−44.464 2 (190)	−44.630 (39)	−42.9
T_{cc}(N)	87.652 2 (162)[d]	87.665 [d]	85.3
χ_{aa}(N)	0.366 (31)	0.322 (41)	
χ_{bb}(N)	−3.833 (37)	−3.809 (47)	
χ_{cc}(N)	3.466 (24)[d]	3.487[d]	
C_{aa}(N)	0.464 8 (81)	0.496 (9)	
C_{bb}(N)	0.098 6 (57)	0.114 (8)	
C_{cc}(N)	0.011 1 (39)	0.022 8 (32)	
a_F(H)	−67.170 2 (116)	−67.182 (36)	63.4
T_{aa}(H)	18.358 5 (221)	18.217 (58)	20.1
T_{bb}(H)	−13.210 8 (247)	−13.05 (9)	−13.0
T_{cc}(H)	−5.147 7 (192)[d]	−5.17[d]	−7.3
T_{ab}(H)	58.5[e]	58.5 (25)	55.7
C_{aa}(H)	0.209 9 (100)	0.253 (8)	
C_{bb}(H)	−0.005 9 (65)		
C_{cc}(H)	−0.023 9 (51)		

[a] Isotropic and anisotropic electron-spin nuclear-spin coupling constants, and nuclear quadrupole and spin-rotation coupling constants. See also footnote to Table 2 and text.
[b] Ref. (*7*), except T_{ab}(H) from Ref. (*19*).
[c] Ref. (*22*).
[d] Derived parameters.
[e] Fixed to value from Ref. (*19*).

TABLE 5
Maximum N and K_a Quantum Numbers, Number of Different Lines, Standard Deviation, and Reduced Standard Deviation in the Final Fit of NH_2

	N_{Max}	$K_{a,Max}$	No_{lines}	rms	dimensionless σ
mmW[a]	5	4	237	90.6 kHz	0.934
MODR[b]	9	3	219	481 kHz	0.819
laser sideband[c]	6	3	35	2.13 MHz	0.715
FT-FIR[d]	13	8	244	$0.559 \cdot 10^{-3}$ cm^{-1}	0.797
overall	13	8	735		0.845

[a] Millimeter to terahertz lines from this work and from Ref. (*7*).
[b] Refs. (*3–5*).
[c] Ref. (*9*); see also section III.
[d] Ref. (*8*).

ACKNOWLEDGMENTS

The work in Köln was supported in part by the Deutsche Forschungsgemeinschaft (DFG) *via* Grant SFB 301 and by special funding from the Science Ministry of the Land Nordrhein-Westfalen. I.M. thanks the Japan Science and Technology Corporation for a Domestic Research Fellowship during his stay at NAIR. S.S. thanks H. Ozeki for helpful discussions.

REFERENCES

1. P. Swing, A. McKellar, and R. Minkowski, *Astrophys. J.* **98,** 142 (1943).
2. E. F. Van Dishoek, D. J. Jansen, P. Schilke, and T. G. Philips, *Astrophys. J.* **416,** L83–L86 (1993).
3. J. M. Cook, G. W. Hills, and R. F. Curl, Jr., *J. Chem. Phys.* **67,** 1450–1461 (1977).
4. J. M. Cook, R. S. Lowe, G. W. Hills, and R. F. Curl, Jr., *J. Chem. Phys.* **68,** 4073–4076 (1978).
5. G. W. Hills and J. M. Cook, *J. Mol. Spectrosc.* **94,** 456–460 (1982).
6. A. Charo, K. V. L. Sastry, E. Herbst, and F. C. De Lucia *Astrophys. J.* **244,** L111–L112 (1993).
7. M. Tonooka, S. Yamamoto, K. Kobayashi, and S. Saito, *J. Chem. Phys.* **106,** 2563–2568 (1997).
8. I. Morino and K. Kawaguchi, *J. Mol. Spectrosc.* **182,** 428–438 (1997).
9. H. Ozeki and S. Saito, *J. Mol. Spectrosc.* **192,** 183–190 (1998).
10. G. Winnewisser, *Vib. Spectrosc.* **8,** 241–253 (1995).
11. G. Winnewisser, S. P. Belov, T. Klaus, and R. Schieder, *J. Mol. Spectrosc.* **184,** 468–472 (1997).
12. T. Klaus, S. Takano, and G. Winnewisser, *Astron. Astrophys.* **322,** L1–L4 (1997).
13. I. Morino, M. Fabian, H. Takeo, and K. M. T. Yamada, *J. Mol. Spectrosc.* **185,** 142–146 (1997).
14. K. Kobayashi, H. Ozeki, S. Saito, M. Tonooka, and S. Yamamoto, *J. Chem. Phys.* **107,** 9289–2568 (1997).
15. (a) R. L. Poynter and H. M. Pickett, *Appl. Opt.* **24,** 2235–2240 (1985); (b) H. M. Pickett, R. L. Poynter, E. A. Cohen, M. L. Delitsky, J. C. Pearson, and H. S. P. Müller, "Submillimeter, Millimeter, and Microwave Line Catalog," JPL Publication 80-23, Revision 4, Pasadena, CA, 1996; (c) H. M. Pickett, R. L. Poynter, E. A. Cohen, M. L. Delitsky, J. C. Pearson, and H. S. P. Müller, *J. Quant. Spectrosc. Radiat. Transfer* **60,** 883–890 (1998).
16. H. M. Pickett, *J. Mol. Spectrosc.* **148,** 371–377 (1991).
17. J. M. Brown and T. J. Sears, *J. Mol. Spectrosc.* **75,** 111–133 (1979).
18. H. S. P. Müller, C. E. Miller, and E. A. Cohen, *J. Chem.Phys.* **107,** 8292–8302 (1997).
19. T. C. Steimle, J. M. Brown, and R. F. Curl, Jr., *J. Chem. Phys.* 73, 2552–2558 (1980).
20. I. Morino and K. Kawaguchi, personal communication.
21. M. Vervloet, unpublished, communicated to H.S.P.M. through L. H. Coudert.
22. K. Funken, B. Engels, and S. D. Peyerimhoff, *Chem. Phys. Lett.* **172,** 180–186 (1990).
23. K. M. T. Yamada, *J. Mol. Spectrosc.* **156,** 512–516 (1992).
24. J. R. Morton and K. F. Preston, *J. Magn. Reson.* **30,** 577–583 (1978).
25. J. M. Brown, S. W. Chalkley, and F. D. Wayne, *Mol. Phys.* **38,** 1521 (1979).